I J C T A, 9(9), 2016, pp. 4071-4080

An Adaptive Unsupervised Segmentation Algorithm Based on Color–Texture (CTEX) Integration

M. Anto Bennet[1], V. Nehru[2], S. Surya[3], R. Sankar[4] and M. Rajasekar[5]

ABSTRACT

This paper presents the development of an unsupervised image segmentation framework that is based on the adaptive inclusion of color and texture in the process of data partition. An important contribution of this work consists of a new formulation for the extraction of color features that evaluates the input image in a multi-space color representation. To achieve this, we have used the opponent characteristics of the RGB and YIQ color spaces where the key component was the inclusion of the Self Organizing Map (SOM) network in the computation of the dominant colors and estimation of the optimal number of clusters in the image. The texture features are computed using a multichannel texture decomposition scheme based on Gabor filtering. The major contribution of this work resides in the adaptive integration of the color and texture features in a compound mathematical descriptor with the aim of identifying the homogenous regions in the image. This integration is performed by a novel adaptive clustering algorithm that enforces the spatial continuity during the data assignment process. A comprehensive qualitative and quantitative performance evaluation has been carried out and the experimental results indicate that the proposed technique is accurate in capturing the color and texture characteristics when applied to complex natural images.

Keywords: Color and Texture, (CTEX), Self Organizing Map (SOM), Adaptive Spatial K-Means Clustering(ASKM).

1. INTRODUCTION

Image segmentation is one of the most investigated subjects in the field of computer vision since it plays a crucial role in the development of high-level image analysis tasks such as object recognition and scene understanding[1,2]. A review of the literature on image segmentation indicates that a significant amount of research has been dedicated to the development of algorithms where the color and texture features where analyzed alone. The early color-texture segmentation algorithms were designed in conjunction with particular applications and they were generally restricted to the segmentation of images that are composed of scenes defined by regions with uniform characteristics. Segmentation of natural images is by far a more difficult task, since natural images exhibit significant in homogeneities in color and texture. Thus the complex characteristics associated with natural mages forced researchers to approach their segmentation using features that locally sample both the color and texture attributes [3, 4]. The use of color and texture information collectively has strong links with the human perception, but the main challenge is the combination of this fundamental image attributes in a coherent color-texture image descriptor. In fact, if we take into consideration that the textures that are present in natural images are often characterized by a high degree of complexity, randomness, and irregularity, the simple inclusion of color and texture is not sufficient and a more appropriate segmentation model would encompass three attributes such as color, texture, and composite elements that are defined by a large mixture of colors [5, 6]. In this paper, we propose a flexible and generic framework (C-Tex) for segmentation of natural images based on color and texture. The developed approach extracts

[1] Professor Department of Electronics and Communication Engineering, Vel Tech, Chennai-600062, *Email: bennetmab@gmail.com*

[2,3,4] Assistant Professors, Department of Computer Science and Engineering,, Vel Tech, Chennai-600062.

[5] Department of CSE, Veltech Multi Tech Engineering College, Chennai-600062, India.

the color features using a multispace adaptive clustering algorithm, while the texture features are calculated using a multichannel texture decomposition scheme. Our segmentation algorithm is unsupervised and its main advantage resides in the fact that the color and texture are included in an adaptive fashion with respect to the image content [7, 8].

2. MATERIALS & METHODS

2.1. Texture Extraction

There has been a widely accepted consensus among vision researchers that filtering an image with a large number of oriented band pass filters such as Gabor represents an optimal approach to analyze textures. Our approach implements a multi-channel texture decomposition and is achieved by filtering the input textured image with a 2-D Gabor filter bank that was initially suggested by Anto Bennet[7] and later applied to texture segmentation by Anto bennet et., al[2].. The 2-D Gabor function that is used to implement the even-symmetric 2-D discrete filters can be written as

$$G_{\sigma}, f, \varphi(x, y) = \exp\left(-\frac{x'^2 + y'^2}{2\sigma^2}\right)\cos\left(2\pi f x' + \varphi\right) \quad (1)$$

Where $x' = x \cos\theta + y \sin\theta$ and $y' = -x \sin\theta + y \cos\theta$

In equation (1), the parameter σ represents the scale of the Gabor filter, θ is the orientation and f is the frequency parameter that controls the number of cycles of the cosine function within the envelope of the 2-D Gaussian (φ is the phase offset and it is usually set to zero to implement 2-D even-symmetric filters).The Gabor filters are band pass filters where the parameters σ, θ, and f that determine the sub-band that is covered by the Gabor filter in the spatial-frequency domain.The parameters of the Gabor filters are chosen to optimize the trade-off between spectral selectivity and the size of the bank of filters. Typically, the

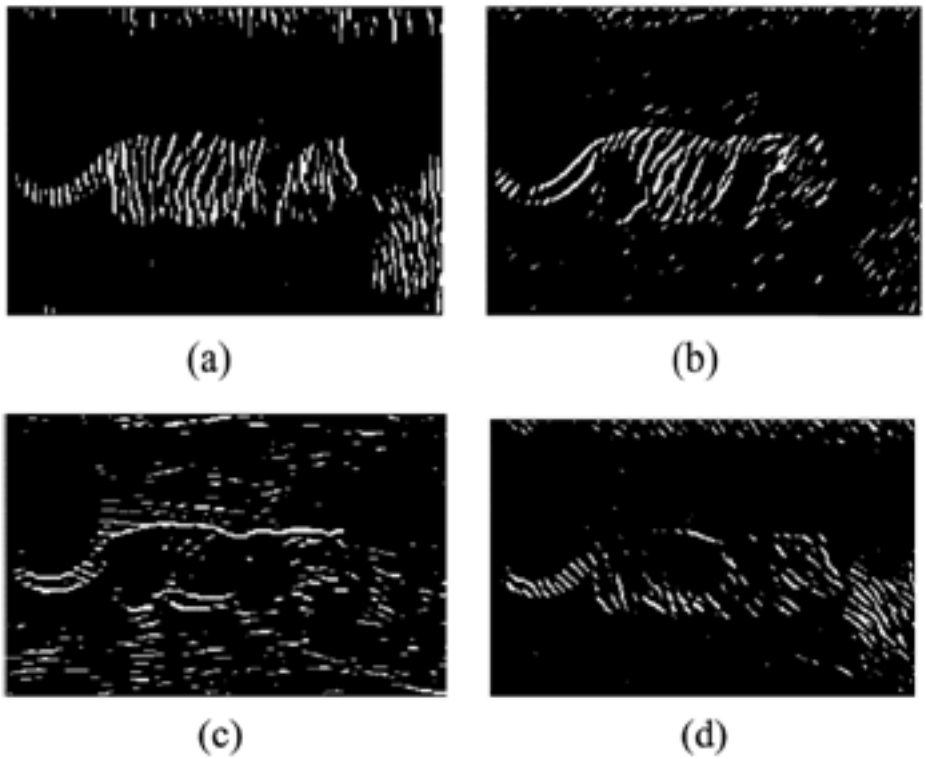

Figure 1: Texture features extracted for the natural image depicted in Figure 7 (i) using Gabor filter with four orientations: (a) 0º, (b) 45º, (c) 90º, and (d) 135º.

central frequencies are selected to be one octave apart and for each central frequency is constructed a set of filters corresponding to four (0^o, 45^o, 90^o,135^o) or six orientations (0^o, 30^o, 60^o, 90^o, 120^o, 150^o). Figure(1) shows the textures features extracted from a natural image, when the Gabor filters are calculated using four orientations.

2.2. Color and Texture Integration

We propose to integrate the color and texture features using a spatially adaptive clustering algorithm. The inclusion of the texture and color features in an adaptive fashion is a difficult task since these attributes are not constant within the image. Thus, the application of standard clustering techniques to complex data such as natural images will lead to over-segmented results since the spatial continuity is not enforced during the space partitioning process. In this paper, our aim is to develop a space-partitioning algorithm that is able to return meaningful results even when applied to complex natural scenes that exhibit large variations in color and texture. To achieve this we propose a new clustering strategy called Adaptive Spatial K-Means Clustering(ASKM) whose implementation can be viewed as a generalization of the K-Means algorithm. The ASKM technique attempts to minimize the errors in the assignment of the data-points into clusters by sampling adaptively the local texture continuity and the local color smoothness in the image. The inputs of the ASKM algorithm are: the color segmented image, the texture images and the final number of clusters k that has been established using the SOM based procedure. The main idea behind ASKM is to minimize an objective function 'J' based on the fitting between the local color and local texture distributions calculated for each data-point (pixel) in the image and the color and texture distributions calculated for each cluster. This approach is motivated by the fact that the color-texture distribution enforces the spatial continuity in the data partitioning process since the color and texture information are evaluated in a local neighborhood for all pixels in the image. The local color distribution for the data-point at location (*x*, y) is calculated as follows:

$$H_C^{sxs} = \bigcup_{b\in[1,k]} h_C^{sxs}(x,y,b)$$

where

$$h_C^{sxs}(x,y,b) = \sum_{p=(x-s/2)}^{x+s/2} \sum_{q=(y-s/2)}^{y+s/2} \delta\big(C(p,q),b\big) \quad (2)$$

and

$$\delta(i,j) = \begin{cases} 1 & i = j \\ 0 & i \neq j \end{cases} \quad (2)$$

Where $H_C^{s\times s}(x,y)$ is the local color distribution calculated from the color segmented *C* image in the neighborhood of size $s \times s$ around the data-point at position (x, y) and k is the number of clusters. In equation (2), the union operator $\cup$ defines the concatenation of the individual histogram bins $h_C^{s\times s}(x,y,b), b\in[1,k]$ that are calculated from the color segmented image C. The local texture distribution $H_T^{s\times s}(x,y)$ is obtained by concatenating the distributions $H_{T_j}^{s\times s}(x,y)$ as follows:

$$(x,y) = \bigcup_{b\in[0,255]} h_{T_j}^{s\,x\,s}(x,y,b)$$

$$h_{T_j}^{s\,x\,s}(x,y,b) = \sum_{p=(x-s/2)}^{x+s/2} \sum_{q=(y-s/2)}^{y+s/2} \delta\big(T_j(p,q),b\big),\ j\in[1,\alpha] \quad (3)$$

$$h_T^{s\,x\,s}(x,y) = \bigcup_{j\in[1,\alpha]} H_{T_j}^{s\,x\,s}(x,y)$$

$$= \left[H_{T_1}^{s\,x\,s}.H_{T_2}^{s\,x\,s}....H_{T_\alpha}^{s\,x\,s} \right] \tag{4}$$

Where T_j is the th Gabor filtered image and α is the total number of texture orientations. In our implementation the pixel values of the texture images T_j are normalized in the range [0,255]. In order to accommodate the color-texture distributions in the clustering process, we replaced the global objective function of the standard K-Means algorithm with the formulation shown in equation (4). The aim of the ASKM algorithm is the minimization of the objective function J that is composed of two distinct terms that impose the local coherence constraints. The first term optimizes the fitting between the local color distribution for the data point under analysis and the global color distribution of each cluster, while the second term optimizes the fitting between the local texture distribution for the same data point with the global texture distribution of each cluster.

$$J = \sum_{x=1}^{width} \sum_{y=1}^{height} \left\{ \sum_{i=1}^{k} \left[\min_{s\in[3x3...25x25]} KS\left(h_C^{s\,x\,s}(x,y).H_C^i\right) + \min_{s\in[3x3...25x25]} KS\left(h_T^{s\,x\,s}(x,y).H_T^i\right) \right] \right\}$$

In equation (14), k is the number of clusters, $s \times s$ defines the size of the local window, $H_C^{s\times s}(x, y)$ and $H_T^{s\times s}(x, y)$ are the local color and the local texture istributions calculated for the pixel at position (x, y) respectively, H_C^i and H_T^i are the color and texture distributions for the cluster with index i respectively. The similarity between the local color-texture distributions and the global color-texture distributions of the clusters is evaluated using the Kolmogorov-Smirnov (KS) metric

$$KS\left(H_a, H_b\right) = \sum_{j\in[0,hist\_size]} \left| \frac{h_a(i)}{n_a} - \frac{h_b(i)}{n_b} \right| \tag{5}$$

Where n_a and n_b are the number of data points in the distributions H_a and H_b, respectively. The main advantage of the KS metric over other similarity metrics such as G-statistic and the Kullback divergence is the fact that the KS metric is normalized and the result of the comparison between the distributions H_a and H_b is bounded in the interval [0, 2]. The fitting between the local color-texture distributions and global color-texture distributions of the clusters is performed adaptively for multiple window sizes in the interval [3 × 3] to [25 × 25]. The evaluation of the fitting between the local and global distributions using a multiresolution approach is motivated by the fact that the color composition of the texture in the image is not constant and the algorithm adjusts the window size until it is achieved the best fit value. It is important to note that the global color-texture distributions H_C^i and H_T^i are updated after each iteration and the algorithm is executed until convergence.

2.3. Gabor filter

A Gabor filter is a linear filter whose impulse response is defined by a harmonic function multiplied by a Gaussian function. Because of the multiplication-convolution property (Convolution theorem), the Fourier transform of a Gabor filter's impulse response is the convolution of the Fourier transform of the harmonic function and the Fourier transform of the Gaussian function.

$$g\left(x, y; \lambda, \theta, \psi, \sigma, \gamma\right) = \exp\left(-\frac{x'^2 + \gamma^2 y'^2}{2\sigma^2} \right) \cos\left(2\pi \frac{x'}{\lambda} + \psi \right)$$

Where

$$x' = x\cos\theta + y\sin\theta_{and}\ \ y' = -x\sin\theta + y\cos\theta$$

In this equation, λ represents the wavelength of the cosine factor, θ represents the orientation of the normal to the parallel stripes of a Gabor function, Ψ is the phase offset, σ is the sigma of the Gaussian envelope and γ is the spatial aspect ratio, and specifies the ellipticity of the support of the Gabor function.Gabor filters are directly related to Gabor wavelets, since they can be designed for number of dilations and rotations. However, in general, expansion is not applied for Gabor wavelets, since this requires computation of biorthogonal wavelets, which may be very time-consuming. Therefore, usually, a filter bank consisting of Gabor filters with various scales and rotations is created. The filters are convolved with the signal, resulting in a so-called Gabor space. This process is closely related to processes in the primary visual cortex. The Gabor space is very useful in e.g., image processing applications such as iris recognition and fingerprint recognition. Relations between activations for a specific spatial location are very distinctive between objects in an image. Furthermore, important activations can be extracted from the Gabor space in order to create a sparse object representation.

3. EXPERIMENTS PERFORMED ON DIFFERENT COLOR IMAGES

A large number of experiments were carried out to assess the performance of the proposed color-texture segmentation framework. These tests were conducted on synthetic and natural image datasets and the results were quantitatively and qualitatively evaluated. The first tests were performed on a dataset of 33 mosaic images and the segmentation results were evaluated by analyzing the errors obtained by computing the displacement between the border pixels of the segmented regions and the region borders in the ground truth data. The second set of experiments was performed on the Berkeley database that is composed of natural images characterized by various degrees of complexity with respect to color and texture information. In order to illustrate the validity of the proposed scheme, we have compared the results returned by the CTex algorithm against those returned by the well-established JSEG color-texture segmentation algorithm developed by Anto bennet et al.,[5]. For the CTex algorithm, the parameters required by the anisotropic diffusion and color segmentation method are discussed in chapter III and IV and are left to the default values in all experiments.The texture features are extracted using Gabor filters and the experiments were conducted using a filter bank that samples the texture in four orientations (0^o, 45^o, 90^o, and 135^o) and the scale and frequency parameters were set to $\sigma = 0$ and $f = 1.5/2''$, respectively.

3.1. Experiments Performed on Mosaic Images

Since the ground truth data associated with complex natural images is difficult to estimate and its extraction is highly influenced by the subjectivity of the human operator, we performed the first set of tests on synthetic data where the ground truth is unambiguous.

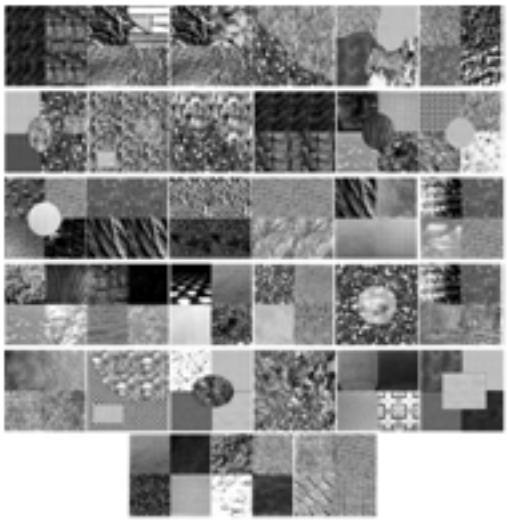

Figure 2: Database of 33 mosaic images

Fig. 2 Database of 33 mosaic images used in our experiments. (These images are labeled from 01 to 33 starting from the upper left image in a raster scan manner)Therefore, we executed the C-Tex and JSEG algorithms on a database of 33 mosaic images (image size 184 × 184) that were created by mixing textures from VisTex and Photoshop databases.The segmentation accuracy of the C-Tex and JSEG algorithms is

Table 1

Image	CTex			JSEG		
	Mean	St_dev	r.m.s	Mean	St_dev	r.m.s
01	0.45	0.52	0.69	0.14	0.35	0.38
02	1.00	1.00	1.42	12.92	22.94	26.33
03	0.68	0.87	1.10	3.36	6.84	7.62
04	0.00	0.11	0.11	0.62	0.69	0.93
05	0.51	0.54	0.75	0.14	0.37	0.40
06	2.15	4.51	5.00	3.19	5.17	6.08
07	1.19	0.90	1.50	1.00	1.33	1.67
08	0.71	0.65	0.97	0.63	0.78	1.00
09	1.36	1.03	1.70	0.66	0.76	1.01
10	1.28	1.92	2.31	0.05	0.23	0.24
11	0.70	0.80	1.07	3.64	6.05	7.06
12	0.78	0.82	1.13	0.38	0.66	0.76
13	0.75	0.68	1.01	1.63	2.36	2.87
14	0.97	0.84	1.28	0.80	1.37	1.59
15	0.35	0.55	0.66	0.34	0.49	0.59
16	0.32	0.46	0.56	0.34	0.48	0.59
17	0.87	0.71	1.12	12.22	22.79	25.86
18	0.96	0.70	1.19	0.65	0.53	0.84
19	0.66	0.83	1.06	0.64	0.68	0.93
20	1.08	1.04	1.50	2.99	4.75	5.62
21	1.28	0.83	1.52	3.28	5.05	6.02
22	0.91	0.48	1.03	0.29	0.52	0.59
23	0.90	0.65	1.12	0.55	0.55	0.78
24	0.99	0.78	1.26	1.01	0.91	1.36
25	0.71	0.96	1.20	0.38	0.53	0.65
26	2.15	1.59	2.67	4.42	6.83	8.13
27	1.03	1.10	1.51	0.13	0.36	0.38
28	2.32	2.36	3.31	2.30	2.74	3.58
29	0.79	0.73	1.08	0.90	1.04	1.38
30	1.00	0.84	1.31	3.54	8.88	9.56
31	0.95	0.89	1.30	0.55	0.68	0.88
32	0.86	0.73	1.13	0.46	0.57	0.74
33	0.74	0.91	1.18	24.54	30.43	39.09
Overall	**0.95**	**0.97**	**1.38**	**2.68**	**4.20**	**5.01**

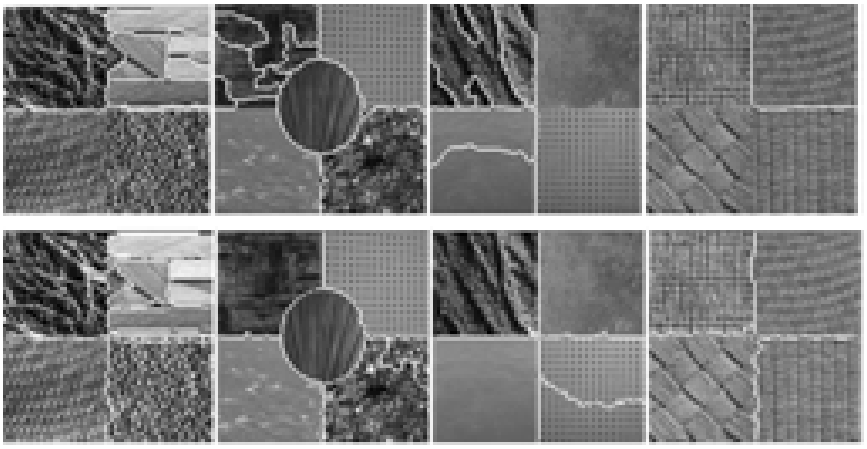

Figure 3: Color texture segmentation

estimated by calculating the Euclidean distances between the pixels situated on the border of the regions present in the segmented results and the border pixels present in the ground truth data. To evaluate the segmentation errors numerically, we calculate the mean, standard deviation and r.m.s errors that measure the border displacement between the ground truth and the segmented results. The experimental data is depicted in Table 1 and shows that the overall mean errors (shown in bold) calculated for C-Tex are smaller than the overall mean errors calculated for the JSEG algorithm.In our experiments, we noticed that the JSEG algorithm performs well in the identification of the image regions defined by similar color-texture properties, but it fails to determine accurately the object borders between the regions that are characterized by similar color compositions. This can be observed in Figure (2), where the images where the JSEG produced the most inaccurate results are shown (images 02, 11, 17, and 33). Point to curve errors between the ground truth and segmented results generated by the ctex and jseg algorithms. The mean and r.m.s errors are given in pixels

Fig 3. Color texture segmentation results when JSEG and C-Tex algorithms where applied to images 02, 11, 17, and 33.First row: JSEG segmentation results. Second row: C-Tex segmentation results. These images are difficult to segment since they are defined by regions with inhomogeneous texture characteristics and the color contrast between them is low. Although the task to segment the images shown in Figure (2) is very challenging, the experimental results in Figure (3) and Table (2) indicate that the C-Tex algorithm is able to produce more consistent segmentation results where the errors in boundary location are significantly smaller than those generated by the JSEG algorithm.

3.2. Experiments Performed on Natural Images

We have tested the proposed C-Tex segmentation algorithm on a large number of complex natural images in order to evaluate its performance with respect to the identification of perceptual color-texture homogenous regions. To achieve this goal, we have applied our technique to Berkeley, McGill, and Outex natural images databases that include images characterized by nonuniform textures, fuzzy borders, and low image contrast.The experiments were conducted to obtain a quantitative and qualitative evaluation of the performance of the C-Tex color-texture segmentation framework. In order to illustrate its validity, we have compared our segmentation results with the ones obtained using the JSEG segmentation algorithm. Although JSEG has a very different computational architecture then C-Tex, this comparison is appropriate since both algorithms include the color and texture attributes in the segmentation process. While the tests conducted on McGill and Outex databases only allowed a qualitative evaluation (since no ground truth data is available), the tests performed on the Berkeley database allowed us to conduct both qualitative and quantitative evaluations since this database provides a set of manual segmentations for each image. In this paper, the

Tabler 2

	$PR\ Index_{mean}$	$PR\ Index_{standard\_deviation}$
JSEG	0.77	0.12
CTex	0.80	0.10

quantitative measurements were carried out using the Probabilistic Rand index (PR). The PR index performs a comparison between the obtained segmentation result and multiple ground-truth segmentations by evaluating the pairwise relationships between pixels.In other words, the PR index measures the agreement between the segmented result and the manually generated ground-truths and takes values in the range (0, 1), where a higher PR value indicates a better match between the segmented result and the ground-truth data.

Performance evaluation of the C-Tex and JSEG algorithms conducted on the berkeley database. The Table2 depicts the mean and the standard deviation of the PR values that are calculated when the C-Tex and JSEG algorithms were applied to all 300 images in the Berkeley database. As it can be observed in Table(2),

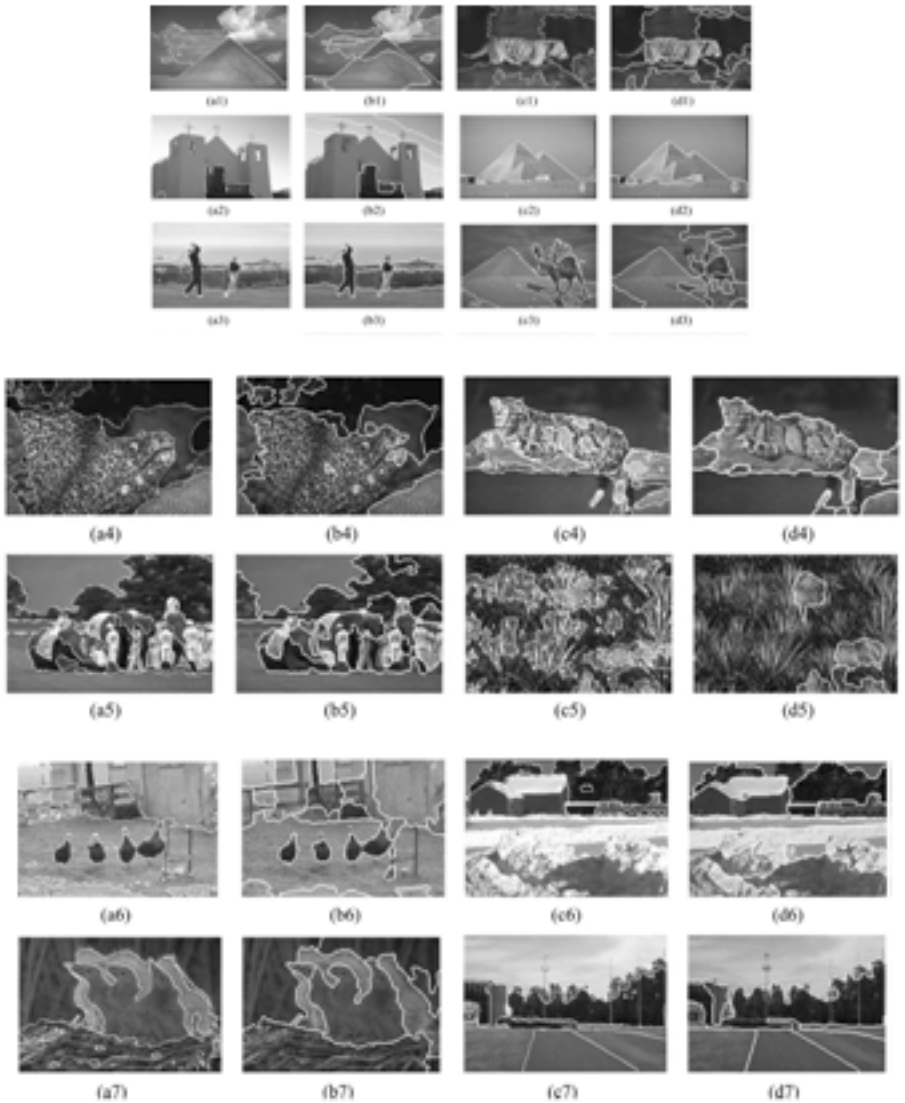

Figure 4: Segmentation of natural images using the C-Tex and JSEG algorithm
• First and third columns (a), (c): C-Tex segmentation results
• Second & fourth columns (b), (d): JSEG segmentation results.

the C-Tex algorithm achieved a mean value of 0.80 while the mean value for JSEG is 0.77.The relative small difference between the quantitative results shown in Table (2) is motivated by the fact that the ground truth images from the Berkeley database are in general under-segmented since the manual annotation of these images was performed to highlight only the perceptual uniform regions. Obviously, this testing scenario favored the JSEG algorithm while the goal of the C-Tex framework is to achieve image segmentation at a high level of image detail.

This can be observed in Figure(4) where a number of segmentation results achieved after the application of C-Tex and JSEG on natural images are illustrated. The results depicted in Figure(4) indicate that although the overall performance of the JSEG algorithm is good, it has difficulty in the identification of the image regions defined by low color contrast (in Fig (4) b3, d3, b4, d4, and d5) and small and narrow details (in Fig (4) d1, b2, b3, d3, and b6). These results also indicate that the C-Tex technique was able to produce consistent results with respect to the border localization of the perceptual regions and the level of image detail (in Figure (4) c1, a2, a3, c3, c5, and a6) and shows better ability than the JSEG algorithm in handling the local in homogeneities in texture and color. The elimination of the small and narrow image details in the segmented results by the JSEG algorithm is caused by two factors. The first is generated by the fact that the region growing that implements the segmentation process performs the seed expansion based only on the 'J' values that sample the texture complexity rather than a texture model and the spatial continuity is evaluated in relative large neighborhoods. The second factor that forces the JSEG algorithm to eliminate the small regions from the segmented output is related to the procedure applied to determine the initial seeds for the region growing algorithm.In the original implementation proposed by Deng and Manjunath the initial seeds correspond to minima of local values and to prevent the algorithm to be trapped in local minima the authors imposed a size criterion for the candidate seed region. In contrast to this approach, the algorithm detailed in this paper (C-Tex) evaluates the color and texture information using explicit models (distributions) and the spatial continuity is enforced during the adaptive integration of the color and texture features in the ASKM framework. As illustrated in equation (5), the ASKM algorithm is able to adjust the size of the local color and texture distributions to the image content and this is an important advantage of our algorithm while the level of image detail in the segmented output is preserved. In Figure(4), segmentation results of natural images from McGill and Outex databases are also included. It is useful to note that some small erroneous regions are generated by our approach that are caused by the incorrect adaptation of the window size (in equation (5)) when dealing with small image regions defined by step transitions in color and texture.This problem can be addressed by applying a post processing merging procedure, but this will lead to a reduction in the level of image detail in the segmented data. However, this problem is difficult to tackle taken into consideration the unsupervised nature of the C-Tex algorithm, but the experimental results indicate that our segmentation framework is robust in determining the main perceptual regions in natural images. One potential solution to address this problem is to include in the ASKM formulation a new regularization term that penalizes the weak discontinuities between adjacent regions by calculating a global spatial continuity cost. This can be achieved by embedding the ASKM process into an energy minimization framework.

4. CONCLUSION

In this work, we presented a new segmentation algorithm where the color and texture features are adaptively evaluated by a clustering strategy that enforces the spatial constraints during the assignment of the data into image regions with uniform texture and color characteristics. The main contribution of this work resides in the development of a novel multispace color segmentation scheme where an unsupervised SOM classifier was applied to extract the dominant colors and estimate the optimal number of clusters in the image. The second strand of the algorithm dealt with the extraction of the texture features using a multichannel decomposition scheme based on Gabor filtering. The inclusion of the color and texture features in a composite

descriptor proved to be effective in the identification of the image regions with homogenous characteristics. The performance of the developed color-texture segmentation algorithm has been quantitatively and qualitatively evaluated on a large number of synthetic and natural images and the experimental results indicate that our algorithm is able to produce accurate segmentation results even when applied to images characterized by low resolution and low contrast.

REFERENCES

[1] Dr. Anto Bennet, M., Sankar Babu G., Natarajan S., "Reverse Room Techniques for Irreversible Data Hiding**"**, Journal of Chemical and Pharmaceutical Sciences 08(03): 469-475, September 2015.

[2] Dr. Anto Bennet, M., Sankaranarayanan S., Sankar Babu G., " Performance & Analysis of Effective Iris Recognition System Using Independent Component Analysis**"**, Journal of Chemical and Pharmaceutical Sciences 08(03): 571-576, August 2015.

[3] Dr. Anto Bennet, M., Sankaranarayanan S., Ashokram S., Dinesh Kumar T. R., "Testing of Error Containment Capability in can Network", International Journal of Applied Engineering Research, Volume 9, Number 19 (2014) pp. 6045-6054

[4] Dr. Anto Bennet, M. "A Novel Effective Refined Histogram For Supervised Texure Classification", International Journal of Computer & Modern Technology, Issue 01, Volume02, pp. 67-73, June 2015.

[5] Dr. Anto Bennet, M., Srinath R., Raisha Banu A., "Development of Deblocking Architectures for block artifact reduction in videos", International Journal of Applied Engineering Research, Volume 10, Number 09 (2015) pp. 6985-6991, April 2015.

[6] Anto Bennet, M. & Jacob Raglend, "Performance Analysis of Filtering Schedule Using Deblocking Filter For The Reduction Of Block Artifacts From MPEQ Compressed Document Images", Journal of Computer Science, vol. 8, no. 9, pp. 1447-1454, 2012.

[7] Anto Bennet, M. & Jacob Raglend, "Performance Analysis of Block Artifact Reduction Scheme Using Pseudo Random Noise Mask Filtering", European Journal of Scientific Research, vol. 66 no. 1, pp. 120-129, 2011.

[8] Anto Bennet, M., Mohan babu, G., Rajasekar, C. & Prakash, P., "Performance and Analysis of Hybrid Algorithm for Blocking and Ringing Artifact Reduction", Journal of Computational and Theoretical nanoscience vol. 12, no. 1, pp. 141-149, 2015.